

## Chapter 37

# Diffraction distraction

(N. Whelan)

**D**IFFRACTION EFFECTS characteristic to scattering off wedges are incorporated into the periodic orbit theory.

### 37.1 Quantum eavesdropping

As noted in chapter 36, the classical mechanics of the helium atom is undefined at the instant of a triple collision. This is a common phenomenon - there is often some singularity or discontinuity in the classical mechanics of physical systems. This discontinuity can even be helpful in classifying the dynamics. The points in phase space which have a past or future at the discontinuity form manifolds which divide the phase space and provide the symbolic dynamics. The general rule is that quantum mechanics smoothes over these discontinuities in a process we interpret as diffraction. We solve the local diffraction problem quantum mechanically and then incorporate this into our global solution. By doing so, we reconfirm the central leitmotif of this treatise: think locally - act globally.

While being a well-motivated physical example, the helium atom is somewhat involved. In fact, so involved that we do not have a clue how to do it. In its place we illustrate the concept of diffractive effects with a pinball game. There are various classes of discontinuities which a billiard can have. There may be a grazing condition such that some trajectories hit a smooth surface while others are unaffected - this leads to the creeping described in chapter 34. There may be a vertex such that trajectories to one side bounce differently from those to the other side. There may be a point scatterer or a magnetic flux line such that we do not know how to continue classical mechanics through the discontinuities. In what follows, we specialize the discussion to the second example - that of vertices or wedges. To further simplify the discussion, we consider the special case of a half line which can be thought of as a wedge of angle zero.

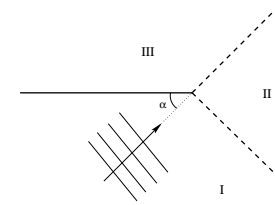


Figure 37.1: Scattering of a plane wave off a half line.

We start by solving the problem of the scattering of a plane wave off a half line (see figure 37.1). This is the local problem whose solution we will use to construct a global solution of more complicated geometries. We define the vertex to be the origin and launch a plane wave at it from an angle  $\alpha$ . What is the total field? This is a problem solved by Sommerfeld in 1896 and our discussion closely follows his.

The total field consists of three parts - the incident field, the reflected field and the diffractive field. Ignoring the third of these for the moment, we see that the space is divided into three regions. In region I there is both an incident and a reflected wave. In region II there is only an incident field. In region III there is nothing so we call this the shadowed region. However, because of diffraction the field does enter this region. This accounts for why you can overhear a conversation if you are on the opposite side of a thick wall but with a door a few meters away. Traditionally such effects have been ignored in semiclassical calculations because they are relatively weak. However, they can be significant.

To solve this problem Sommerfeld worked by analogy with the full line case, so let us briefly consider that much simpler problem. There we know that the problem can be solved by images. An incident wave of amplitude  $A$  is of the form

$$v(r, \psi) = A e^{-ikr \cos \psi} \quad (37.1)$$

where  $\psi = \phi - \alpha$  and  $\phi$  is the angular coordinate. The total field is then given by the method of images as

$$v_{\text{tot}} = v(r, \phi - \alpha) - v(r, \phi + \alpha), \quad (37.2)$$

where the negative sign ensures that the boundary condition of zero field on the line is satisfied.

Sommerfeld then argued that  $v(r, \psi)$  can also be given a complex integral representation

$$v(r, \psi) = A \int_C d\beta f(\beta, \psi) e^{-ikr \cos \beta}. \quad (37.3)$$

This is certainly correct if the function  $f(\beta, \psi)$  has a pole of residue  $1/2\pi i$  at  $\beta =$

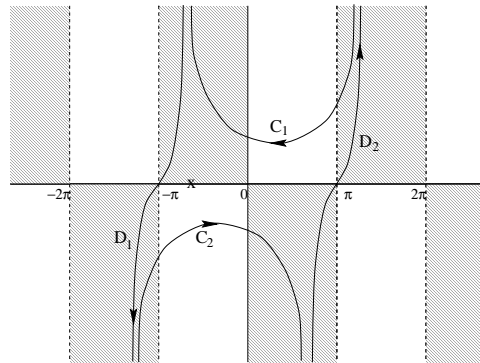


**Figure 37.2:** The contour in the complex  $\beta$  plane. The pole is at  $\beta = -\psi$  (marked by  $\times$  in the figure) and the integrand approaches zero in the shaded regions as the magnitude of the imaginary part of  $\beta$  approaches infinity.

$-\psi$  and if the contour  $C$  encloses that pole. One choice is

$$f(\beta, \psi) = \frac{1}{2\pi} \frac{e^{i\beta}}{e^{i\beta} - e^{-i\psi}}. \quad (37.4)$$

(We choose the pole to be at  $\beta = -\psi$  rather than  $\beta = \psi$  for reasons discussed later.) One valid choice for the contour is shown in figure 37.2. This encloses the pole and vanishes as  $|\text{Im}\beta| \rightarrow \infty$  (as denoted by the shading). The sections  $D_1$  and  $D_2$  are congruent because they are displaced by  $2\pi$ . However, they are traversed in an opposite sense and cancel, so our contour consists of just the sections  $C_1$  and  $C_2$ . The motivation for expressing the solution in this complicated manner should become clear soon.

What have we done? We extended the space under consideration by a factor of two and then constructed a solution by assuming that there is also a source in the unphysical space. We superimpose the solutions from the two sources and at the end only consider the solution in the physical space to be meaningful. Furthermore, we expressed the solution as a contour integral which reflects the  $2\pi$  periodicity of the problem. The half line scattering problem follows by analogy.

Whereas for the full line the field is periodic in  $2\pi$ , for the half line it is periodic in  $4\pi$ . This can be seen by the fact that the field can be expanded in a series of the form  $\{\sin(\phi/2), \sin(\phi), \sin(3\phi/2), \dots\}$ . As above, we extend the space by thinking of it as two sheeted. The physical sheet is as shown in figure 37.1 and the unphysical sheet is congruent to it. The sheets are glued together along the half line so that a curve in the physical space which intersects the half line is continued in the unphysical space and vice-versa. The boundary conditions are that the total field is zero on both faces of the half line (which are physically distinct boundary conditions) and that as  $r \rightarrow \infty$  the field is composed solely of plane waves and outgoing circular waves of the form  $g(\phi)\exp(ikr)/\sqrt{kr}$ . This last condition is a result of Huygens' principle.

We assume that the complete solution is also given by the method of images

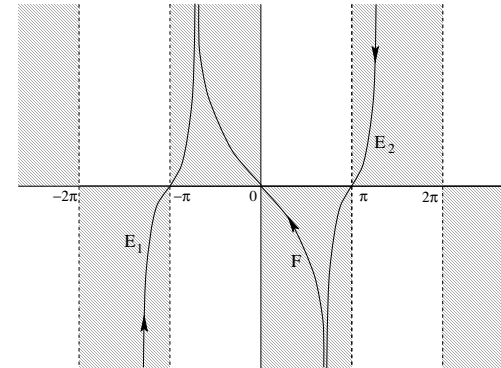


**Figure 37.3:** The contour used to evaluate the diffractive field after the contribution of possible poles has been explicitly evaluated. The curve  $F$  is traversed twice in opposite directions and has no net contribution.

as

$$v_{\text{tot}} = u(r, \phi - \alpha) - u(r, \phi + \alpha). \quad (37.5)$$

where  $u(r, \psi)$  is a  $4\pi$ -periodic function to be determined. The second term is interpreted as an incident field from the unphysical space and the negative sign guarantees that the solution vanishes on both faces of the half line. Sommerfeld then made the ansatz that  $u$  is as given in equation (37.3) with the same contour  $C_1 + C_2$  but with the  $4\pi$  periodicity accounted for by replacing equation (37.4) with

$$f(\beta, \psi) = \frac{1}{4\pi} \frac{e^{i\beta/2}}{e^{i\beta/2} - e^{-i\psi/2}}. \quad (37.6)$$

(We divide by  $4\pi$  rather than  $2\pi$  so that the residue is properly normalized.) The integral (37.3) can be thought of as a linear superposition of an infinity of plane waves each of which satisfies the Helmholtz equation  $(\nabla^2 + k^2)v = 0$ , and so their combination also satisfies the Helmholtz equation. We will see that the diffracted field is an outgoing circular wave; this being a result of choosing the pole at  $\beta = -\psi$  rather than  $\beta = \psi$  in equation (37.4). Therefore, this ansatz is a solution of the equation and satisfies all boundary conditions and therefore constitutes a valid solution. By uniqueness this is the only solution.

In order to further understand this solution, it is useful to massage the contour. Depending on  $\phi$  there may or may not be a pole between  $\beta = -\pi$  and  $\beta = \pi$ . In region I, both functions  $u(r, \phi \pm \alpha)$  have poles which correspond to the incident and reflected waves. In region II, only  $u(r, \phi - \alpha)$  has a pole corresponding to the incident wave. In region III there are no poles because of the shadow. Once we have accounted for the geometrical waves (i.e., the poles), we extract the diffracted waves by saddle point analysis at  $\beta = \pm\pi$ . We do this by deforming the contours  $C$  so that they go through the saddles as shown in figure 37.2.

Contour  $C_1$  becomes  $E_2 + F$  while contour  $C_2$  becomes  $E_1 - F$  where the minus sign indicates that it is traversed in a negative sense. As a result,  $F$  has no net contribution and the contour consists of just  $E_1$  and  $E_2$ .

As a result of these machinations, the curves  $E$  are simply the curves  $D$  of figure 37.2 but with a reversed sense. Since the integrand is no longer  $2\pi$  periodic, the contributions from these curves no longer cancel. We evaluate both stationary phase integrals to obtain

$$u(r, \psi) \approx -A \frac{e^{i\pi/4}}{\sqrt{8\pi}} \sec(\psi/2) \frac{e^{ikr}}{\sqrt{kr}} \quad (37.7)$$

so that the total diffracted field is

$$v_{\text{diff}} = -A \frac{e^{i\pi/4}}{\sqrt{8\pi}} \left( \sec\left(\frac{\phi - \alpha}{2}\right) - \sec\left(\frac{\phi + \alpha}{2}\right) \right) \frac{e^{ikr}}{\sqrt{kr}}. \quad (37.8)$$

Note that this expression breaks down when  $\phi \pm \alpha = \pi$ . These angles correspond to the borders among the three regions of figure 37.1 and must be handled more carefully - we can not do a stationary phase integral in the vicinity of a pole. However, the integral representation (37.3) and (37.6) is uniformly valid.

[exercise 37.1]

We now turn to the simple task of translating this result into the language of semiclassical Green's functions. Instead of an incident plane wave, we assume a source at point  $x'$  and then compute the resulting field at the receiver position  $x$ . If  $x$  is in region I, there is both a direct term, and a reflected term, if  $x$  is in region II there is only a direct term and if  $x$  is in region III there is neither. In any event these contributions to the semiclassical Green's function are known since the free space Green's function between two points  $x_2$  and  $x_1$  is

$$G_{\text{f}}(x_2, x_1, k) = -\frac{i}{4} H_0^{(+)}(kd) \approx -\frac{1}{\sqrt{8\pi kd}} \exp\{i(kd + \pi/4)\}, \quad (37.9)$$

where  $d$  is the distance between the points. For a reflection, we need to multiply by  $-1$  and the distance is the length of the path via the reflection point. Most interesting for us, there is also a diffractive contribution to the Green's function. In equation (37.8), we recognize that the coefficient  $A$  is simply the intensity at the origin if there were no scatterer. This is therefore replaced by the Green's function to go from the source to the vertex which we label  $x_V$ . Furthermore, we recognize that  $\exp(ikr)/\sqrt{kr}$  is, within a proportionality constant, the semiclassical Green's function to go from the vertex to the receiver.

Collecting these facts, we say

$$G_{\text{diff}}(x, x', k) = G_{\text{f}}(x, x_V, k) d(\theta, \theta') G_{\text{f}}(x_V, x', k), \quad (37.10)$$

where, by comparison with equations (37.8) and (37.9), we have

$$d(\theta, \theta') = \sec\left(\frac{\theta - \theta'}{2}\right) - \sec\left(\frac{\theta + \theta'}{2}\right). \quad (37.11)$$

Here  $\theta'$  is the angle to the source as measured from the vertex and  $\theta$  is the angle to the receiver. They were denoted as  $\alpha$  and  $\phi$  previously. Note that there is a symmetry between the source and receiver as we expect for a time-reversal invariant process. Also the diffraction coefficient  $d$  does not depend on which face of the half line we use to measure the angles. As we will see, a very important property of  $G_{\text{diff}}$  is that it is a simple multiplicative combination of other semiclassical Green's functions.

[exercise 37.2]

We now recover our classical perspective by realizing that we can still think of classical trajectories. In calculating the quantum Green's function, we sum over the contributions of various paths. These include the classical trajectories which connect the points and also paths which connect the points via the vertex. These have different weights as given by equations (37.9) and (37.10) but the concept of summing over classical paths is preserved.

For completeness, we remark that there is an exact integral representation for the Green's function in the presence of a wedge of arbitrary opening angle [15]. It can be written as

$$G(x, x', k) = g(r, r', k, \theta' - \theta) - g(r, r', k, \theta' + \theta) \quad (37.12)$$

where  $(r, \theta)$  and  $(r', \theta')$  are the polar coordinates of the points  $x$  and  $x'$  as measured from the vertex and the angles are measured from either face of the wedge. The function  $g$  is given by

$$g(r, r', k, \psi) = \frac{i}{8\pi\nu} \int_{C_1+C_2} d\beta \frac{H_0^{(+)}(k\sqrt{r^2 + r'^2 - 2rr'\cos\beta})}{1 - \exp(i\frac{\beta+\psi}{\nu})} \quad (37.13)$$

where  $\nu = \gamma/\pi$  and  $\gamma$  is the opening angle of the wedge. (ie  $\gamma = 2\pi$  in the case of the half plane). The contour  $C_1 + C_2$  is the same as shown in figure 37.2.

The poles of this integral give contributions which can be identified with the geometric paths connecting  $x$  and  $x'$ . The saddle points at  $\beta = \pm\pi$  give contributions which can be identified with the diffractive path connecting  $x$  and  $x'$ . The saddle point analysis allows us to identify the diffraction constant as

$$d(\theta, \theta') = -\frac{4 \sin \frac{\pi}{\nu}}{\nu} \frac{\sin \frac{\theta}{\nu} \sin \frac{\theta'}{\nu}}{\left(\cos \frac{\pi}{\nu} - \cos \frac{\theta+\theta'}{\nu}\right) \left(\cos \frac{\pi}{\nu} - \cos \frac{\theta-\theta'}{\nu}\right)}, \quad (37.14)$$

which reduces to (37.11) when  $\nu = 2$ . Note that the diffraction coefficient vanishes identically if  $\nu = 1/n$  where  $n$  is any integer. This corresponds to wedge angles of  $\gamma = \pi/n$  (eg.  $n=1$  corresponds to a full line and  $n=2$  corresponds to a right angle). This demonstration is limited by the fact that it came from a leading order asymptotic expansion but the result is quite general. For such wedge angles, we can use the method of images (we will require  $2n - 1$  images in addition to the actual source point) to obtain the Green's function and there is no diffractive

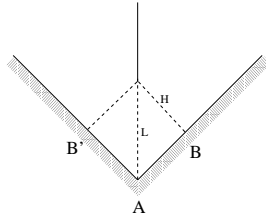


**Figure 37.4:** The billiard considered here. The dynamics consists of free motion followed by specular reflections off the faces. The top vertex induces diffraction while the bottom one is a right angle and induces two specular geometric reflections.

contribution to any order. Classically this corresponds to the fact that for such angles, there is no discontinuity in the dynamics. Trajectories going into the vertex can be continued out of them unambiguously. This meshes with the discussion in the introduction where we argued that diffractive effects are intimately linked with classical discontinuities.

The integral representation is also useful because it allows us to consider geometries such that the angles are near the optical boundaries or the wedge angle is close to  $\pi/n$ . For these geometries the saddle point analysis leading to (37.14) is invalid due to the existence of a nearby pole. In that event, we require a more sophisticated asymptotic analysis of the full integral representation.

## 37.2 An application

Although we introduced diffraction as a correction to the purely classical effects; it is instructive to consider a system which can be quantized solely in terms of periodic diffractive orbits. Consider the geometry shown in figure 37.4. The classical mechanics consists of free motion followed by specular reflections off faces. The upper vertex is a source of diffraction while the lower one is a right angle and induces no diffraction. This is an open system, there are no bound states - only scattering resonances. However, we can still test the effectiveness of the theory in predicting them. Formally, scattering resonances are the poles of the scattering  $S$  matrix and by an identity of Balian and Bloch are also poles of the quantum Green's function. We demonstrate this fact in chapter 34 for 2-dimensional scatterers. The poles have complex wavenumber  $k$ , as for the 3-disk problem.

Let us first consider how diffractive orbits arise in evaluating the trace of  $G$  which we call  $g(k)$ . Specifying the trace means that we must consider all paths which close on themselves in the configuration space while stationary phase arguments for large wavenumber  $k$  extract those which are periodic - just as for classical trajectories. In general,  $g(k)$  is given by the sum over all diffractive and geometric orbits. The contribution of the simple diffractive orbit labeled  $\gamma$  shown in figure 37.5 to  $g(k)$  is determined as follows.

We consider a point  $P$  just a little off the path and determine the semiclassical Green's function to return to  $P$  via the vertex using (37.9) and (37.10). To leading order in  $y$  the lengths of the two geometric paths connecting  $P$  and  $V$  are  $d_{\pm} =$

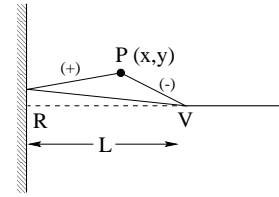


**Figure 37.5:** The dashed line shows a simple periodic diffractive orbit  $\gamma$ . Between the vertex  $V$  and a point  $P$  close to the orbit there are two geometric legs labeled  $\pm$ . The origin of the coordinate system is chosen to be at  $R$ .

$(L \pm x) + y^2 / (L \pm x)^2 / 2$  so that the phase factor  $ik(d_+ + d_-)$  equals  $2ikL + ik y^2 / (L^2 - x^2)$ . The trace integral involves integrating over all points  $P$  and is

$$g_{\gamma}(k) \approx -2d_{\gamma} \frac{e^{i(2kL + \pi/2)}}{8\pi k} \int_0^L \frac{dx}{\sqrt{L^2 - x^2}} \int_{-\infty}^{\infty} dy e^{i(ky^2 \frac{L}{L^2 - x^2})}. \quad (37.15)$$

We introduced an overall negative sign to account for the reflection at the hard wall and multiplied by 2 to account for the two traversal senses,  $VRPV$  and  $VPRV$ . In the spirit of stationary phase integrals, we have neglected the  $y$  dependence everywhere except in the exponential. The diffraction constant  $d_{\gamma}$  is the one corresponding to the diffractive periodic orbit. To evaluate the  $y$  integral, we use the identity

$$\int_{-\infty}^{\infty} d\xi e^{i a \xi^2} = e^{i\pi/4} \sqrt{\frac{\pi}{a}}, \quad (37.16)$$

and thus obtain a factor which precisely cancels the  $x$  dependence in the  $x$  integral. This leads to the rather simple result

$$g_{\gamma} \approx -\frac{il_{\gamma}}{2k} \left\{ \frac{d_{\gamma}}{\sqrt{8\pi k l_{\gamma}}} \right\} e^{i(k l_{\gamma} + \pi/4)} \quad (37.17)$$

where  $l_{\gamma} = 2L$  is the length of the periodic diffractive orbit. A more sophisticated analysis of the trace integral has been done [6] using the integral representation (37.13). It is valid in the vicinity of an optical boundary and also for wedges with opening angles close to  $\pi/n$ .

Consider a periodic diffractive orbit with  $n_{\gamma}$  reflections off straight hard walls and  $\mu_{\gamma}$  diffractions each with a diffraction constant  $d_{\gamma,j}$ . The total length of the orbit  $L_{\gamma} = \sum l_{\gamma,j}$  is the sum of the various diffractive legs and  $l_{\gamma}$  is the length of the corresponding prime orbit. For such an orbit, (37.17) generalizes to

$$g_{\gamma}(k) = -\frac{il_{\gamma}}{2k} \left\{ \prod_{j=1}^{\mu_{\gamma}} \frac{d_{\gamma,j}}{\sqrt{8\pi k l_{\gamma,j}}} \right\} \exp \{i(kL_{\gamma} + n_{\gamma}\pi - 3\mu_{\gamma}\pi/4)\}. \quad (37.18)$$

[exercise 37.3]

Each diffraction introduces a factor of  $1/\sqrt{k}$  and multi-diffractive orbits are thereby suppressed.

If the orbit  $\gamma$  is prime then  $L_\gamma = l_\gamma$ . If  $\gamma$  is the  $r$ 'th repeat of a prime orbit  $\beta$  we have  $L_\gamma = rl_\beta$ ,  $n_\gamma = rp_\beta$  and  $\mu_\gamma = r\sigma_\beta$ , where  $l_\beta$ ,  $p_\beta$  and  $\sigma_\beta$  all refer to the prime orbit. We can then write

$$g_\gamma = g_{\beta,r} = -\frac{il_\beta r}{2k} t_\beta^r \quad (37.19)$$

where

$$t_\beta = \left\{ \prod_{j=1}^{\sigma_\beta} \frac{d_{\beta,j}}{\sqrt{8\pi k l_{\beta,j}}} \right\} \exp\{i(kl_\beta + p_\beta\pi - 3\sigma_\beta\pi/4)\}. \quad (37.20)$$

It then makes sense to organize the sum over diffractive orbits as a sum over the prime diffractive orbits and a sum over the repetitions

$$g_{\text{diff}}(k) = \sum_\beta \sum_{r=1}^{\infty} g_{\beta,r} = -\frac{i}{2k} \sum_\beta l_\beta \frac{t_\beta}{1-t_\beta}. \quad (37.21)$$

We cast this as a logarithmic derivative (17.7) by noting that  $\frac{dt_\beta}{dk} = il_\beta t_\beta - \sigma_\beta l_\beta / 2k$  and recognizing that the first term dominates in the semiclassical limit. It follows that

$$g_{\text{diff}}(k) \approx \frac{1}{2k} \frac{d}{dk} \left\{ \ln \prod_\beta (1-t_\beta) \right\}. \quad (37.22)$$

In the case that there are only diffractive periodic orbits - as in the geometry of figure 37.4 - the poles of  $g(k)$  are the zeros of a dynamical zeta function

$$1/\zeta(k) = \prod_\beta (1-t_\beta). \quad (37.23)$$

For geometric orbits, this function would be evaluated with a cycle expansion as discussed in chapter 18. However, here we can use the multiplicative nature of the weights  $t_\beta$  to find a closed form representation of the function using a Markov graph, as in sect. 10.4.1. This multiplicative property of the weights follows from the fact that the diffractive Green's function (37.10) is multiplicative in segment semiclassical Green's functions, unlike the geometric case.

There is a reflection symmetry in the problem which means that all resonances can be classified as even or odd. Because of this, the dynamical zeta function factorizes as  $1/\zeta = 1/\zeta_+ \zeta_-$  (as explained in sects. 19.5 and 19.1.1) and we determine  $1/\zeta_+$  and  $1/\zeta_-$  separately using the ideas of symmetry decomposition of chapter 19.

In the Markov graph shown in figure 37.6, we enumerate all processes. We start by identifying the fundamental domain as just the right half of figure 37.4.

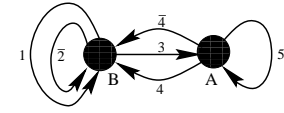


Figure 37.6: The two-node Markov graph with all the diffractive processes connecting the nodes.

There are two nodes which we call  $A$  and  $B$ . To get to another node from  $B$ , we can diffract (always via the vertex) in one of three directions. We can diffract back to  $B$  which we denote as process 1. We can diffract to  $B$ 's image point  $B'$  and then follow this by a reflection. This process we denote as  $\bar{2}$  where the bar indicates that it involves a reflection. Third, we can diffract to node  $A$ . Starting at  $A$  we can also diffract to a node in three ways. We can diffract to  $B$  which we denote as 4. We can diffract to  $B'$  followed by a reflection which we denote as  $\bar{4}$ . Finally, we can diffract back to  $A$  which we denote as process 5. Each of these processes has its own weight which we can determine from the earlier discussion. First though, we construct the dynamical zeta functions.

The dynamical zeta functions are determined by enumerating all closed loops which do not intersect themselves in figure 37.6. We do it first for  $1/\zeta_+$  because that is simpler. In that case, the processes with bars are treated on an equal footing as the others. Appealing back to sect. 19.5 we find

$$\begin{aligned} 1/\zeta_+ &= 1 - t_1 - t_2 - t_5 - t_3 t_4 - t_3 t_{\bar{4}} + t_5 t_1 + t_5 t_2, \\ &= 1 - (t_1 + t_2 + t_5) - 2t_3 t_4 + t_5(t_1 + t_2) \end{aligned} \quad (37.24)$$

where we have used the fact that  $t_4 = t_{\bar{4}}$  by symmetry. The last term has a positive sign because it involves the product of shorter closed loops. To calculate  $1/\zeta_-$ , we note that the processes with bars have a relative negative sign due to the group theoretic weight. Furthermore, process 5 is a boundary orbit (see sect. 19.3.1) and only affects the even resonances - the terms involving  $t_5$  are absent from  $1/\zeta_-$ . The result is

$$\begin{aligned} 1/\zeta_- &= 1 - t_1 + t_2 - t_3 t_4 + t_3 t_{\bar{4}}, \\ &= 1 - (t_1 - t_2). \end{aligned} \quad (37.25)$$

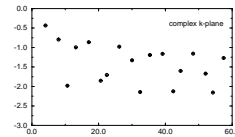
Note that these expressions have a finite number of terms and are not in the form of a curvature expansion, as for the 3-disk problem. [exercise 37.4]

It now just remains to fix the weights. We use equation (37.20) but note that each weight involves just one diffraction constant. It is then convenient to define the quantities

$$u_A^2 = \frac{\exp\{i(2kL + 2\pi)\}}{\sqrt{16\pi k L}} \quad u_B^2 = \frac{\exp\{i(2kH + \pi)\}}{\sqrt{16\pi k H}}. \quad (37.26)$$

The lengths  $L$  and  $H = L/\sqrt{2}$  are defined in figure 37.4; we set  $L = 1$  throughout. Bouncing inside the right angle at  $A$  corresponds to two specular reflections so that

**Figure 37.7:** The even resonances of the wedge scatterer of figure 37.4 plotted in the complex  $k$ -plane, with  $L = 1$ . The exact resonances are represented as circles and their semiclassical approximations as crosses.



$p = 2$ . We therefore explicitly include the factor  $\exp(i2\pi)$  in (37.26) although it is trivially equal to one. Similarly, there is one specular reflection at point  $B$  giving  $p = 1$  and therefore a factor of  $\exp(i\pi)$ . We have defined  $u_A$  and  $u_B$  because, together with some diffraction constants, they can be used to construct all of the weights. Altogether we define four diffraction coefficients:  $d_{AB}$  is the constant corresponding to diffracting from  $B$  to  $A$  and is found from (37.11) with  $\theta' = 3\pi/4$  and  $\theta = \pi$  and equals  $2 \sec(\pi/8) \approx 2.165$ . With analogous notation, we have  $d_{AA}$  and  $d_{BB} = d_{B'B}$  which equal 2 and  $1 + \sqrt{2}$  respectively.  $d_{ij} = d_{ji}$  due to the Green's function symmetry between source and receiver referred to earlier. Finally, there is the diffractive phase factor  $s = \exp(-i3\pi/4)$  each time there is a diffraction. The weights are then as follows:

$$\begin{aligned} t_1 = sd_{BB}u_B^2 \quad t_2 = sd_{B'B}u_B^2 \quad t_3 = t_4 = t_4 = sd_{AB}u_Au_B \\ t_5 = sd_{AA}u_A^2. \end{aligned} \quad (37.27)$$

Each weight involves two  $u$ 's and one  $d$ . The  $u$ 's represent the contribution to the weight from the paths connecting the nodes to the vertex and the  $d$  gives the diffraction constant connecting the two paths.

The equality of  $d_{BB}$  and  $d_{B'B}$  implies that  $t_1 = t_2$ . From (37.25) this means that there are no odd resonances because 1 can never equal 0. For the even resonances equation (37.24) is an implicit equation for  $k$  which has zeros shown in figure 37.7.

For comparison we also show the result from an exact quantum calculation. The agreement is very good right down to the ground state - as is so often the case with semiclassical calculations. In addition we can use our dynamical zeta function to find arbitrarily high resonances and the results actually improve in that limit. In the same limit, the exact numerical solution becomes more difficult to find so the dynamical zeta function approximation is particularly useful in that case.

[exercise 37.5]

In general a system will consist of both geometric and diffractive orbits. In that case, the full dynamical zeta function is the product of the geometric zeta function and the diffractive one. The diffractive weights are typically smaller by order  $O(1/\sqrt{k})$  but for small  $k$  they can be numerically competitive so that there is a significant diffractive effect on the low-lying spectrum. It might be expected that higher in the spectrum, the effect of diffraction is weaker due to the decreasing weights. However, it should be pointed out that an analysis of the situation for creeping diffraction [7] concluded that the diffraction is actually *more* important higher in the spectrum due to the fact that an ever greater fraction of the orbits need to be corrected for diffractive effects. The equivalent analysis has not been done for edge diffraction but a similar conclusion can probably be expected.

To conclude this chapter, we return to the opening paragraph and discuss the possibility of doing such an analysis for helium. The important point which allowed us to successfully analyze the geometry of figure 37.4 is that when a trajectory is near the vertex, we can extract its diffraction constant without reference to the other facets of the problem. We say, therefore, that this is a “local” analysis for the purposes of which we have “turned off” the other aspects of the problem, namely sides  $AB$  and  $AB'$ . By analogy, for helium, we would look for some simpler description of the problem which applies near the three body collision. However, there is nothing to “turn off.” The local problem is just as difficult as the global one since they are precisely the same problem, just related by scaling. Therefore, it is not at all clear that such an analysis is possible for helium.

## Résumé

In this chapter we have discovered new types of periodic orbits contributing to the semiclassical traces and determinants. Unlike the periodic orbits we had seen so far, these are not true classical orbits. They are generated by singularities of the scattering potential. In these singular points the classical dynamics has no unique definition, and the classical orbits hitting the singularities can be continued in many different directions. While the classical mechanics does not know which way to go, quantum mechanics solves the dilemma by allowing us to continue in all possible directions. The likelihoods of different paths are given by the quantum mechanical weights called diffraction constants. The total contribution to a trace from such orbit is given by the product of transmission amplitudes between singularities and diffraction constants of singularities. The weights of diffractive periodic orbits are at least of order  $1/\sqrt{k}$  weaker than the weights associated with classically realizable orbits, and their contribution at large energies is therefore negligible. Nevertheless, they can strongly influence the low lying resonances or energy levels. In some systems, such as the  $N$  disk scattering the diffraction effects do not only perturb semiclassical resonances, but can also create new low energy resonances. Therefore it is always important to include the contributions of diffractive periodic orbits when semiclassical methods are applied at low energies.

## Commentary

**Remark 37.1** Classical discontinuities. Various classes of discontinuities for billiard and potential problems discussed in the literature:

- a grazing condition such that some trajectories hit a smooth surface while others are unaffected, refs. [1, 2, 3, 7]
- a vertex such that trajectories to one side bounce differently from those to the other side, refs. [2, 4, 5, 8, 9].
- a point scatterer [10, 11] or a magnetic flux line [12, 13] such that we do not know how to continue classical mechanics through the discontinuities.



**Remark 37.2 Geometrical theory of diffraction.** In the above discussion we borrowed heavily from the ideas of Keller who was interested in extending the geometrical ray picture of optics to cases where there is a discontinuity. He maintained that we could hang onto that ray-tracing picture by allowing rays to strike the vertex and then leave at any angle with amplitude (37.8). Both he and Sommerfeld were thinking of optics and not quantum mechanics and they did not phrase the results in terms of semiclassical Green's functions but the essential idea is the same.

**Remark 37.3 Generalizations** Consider the effect of replacing our half line by a wedge of angle  $\gamma_1$  and the right angle by an arbitrary angle  $\gamma_2$ . If  $\gamma_2 > \gamma_1$  and  $\gamma_2 \geq \pi/2$  this is an open problem whose solution is given by equations (37.24) and (37.25) (there will then be odd resonances) but with modified weights reflecting the changed geometry [8]. (For  $\gamma_2 < \pi/2$ , more diffractive periodic orbits appear and the dynamical zeta functions are more complicated but can be calculated with the same machinery.) When  $\gamma_2 = \gamma_1$ , the problem in fact has bound states [21, 22]. This last case has been of interest in studying electron transport in mesoscopic devices and in microwave waveguides. However we can not use our formalism as it stands because the diffractive periodic orbits for this geometry lie right on the border between illuminated and shadowed regions so that equation (37.7) is invalid. Even the more uniform derivation of [6] fails for that particular geometry, the problem being that the diffractive orbit actually lives on the edge of a family of geometric orbits and this makes the analysis still more difficult.

**Remark 37.4 Diffractive Green's functions.** The result (37.17) is proportional to the length of the orbit times the semiclassical Green's function (37.9) to go from the vertex back to itself along the classical path. The multi-diffractive formula (37.18) is proportional to the total length of the orbit times the product of the semiclassical Green's functions to go from one vertex to the next along classical paths. This result generalizes to any system — either a pinball or a potential — which contains point singularities such that we can define a diffraction constant as above. The contribution to the trace of the semiclassical Green's function coming from a diffractive orbit which hits the singularities is proportional to the total length (or period) of the orbit times the product of semiclassical Green's functions in going from one singularity to the next. This result first appeared in reference [2] and a derivation can be found in reference [9]. A similar structure also exists for creeping [2].

**Remark 37.5 Diffractive orbits for hydrogenic atoms.** An analysis in terms of diffractive orbits has been made in a different atomic physics system, the response of hydrogenic atoms to strong magnetic fields [23]. In these systems, a single electron is highly excited and takes long traversals far from the nucleus. Upon returning to a hydrogen nucleus, it is re-ejected with the reversed momentum as discussed in chapter 36. However, if the atom is not hydrogen but sodium or some other atom with one valence electron, the returning electron feels the charge distribution of the core electrons and not just the charge of the nucleus. This so-called quantum defect induces scattering in addition to the classical re-ejection present in the hydrogen atom. (In this case the local analysis consists of neglecting the magnetic field when the trajectory is near the nucleus.) This is formally similar to the vertex which causes both specular reflection and diffraction. There is then additional structure in the Fourier transform of the quantum spectrum corresponding to the induced diffractive orbits, and this has been observed experimentally [24].

## Exercises

37.1. **Stationary phase integral.** Evaluate the two stationary phase integrals corresponding to contours  $E_1$  and  $E_2$  of figure 37.3 and thereby verify (37.7).

(N. Whelan)

37.2. **Scattering from a small disk** Imagine that instead of a wedge, we have a disk whose radius  $a$  is much smaller than the typical wavelengths we are considering. In that limit, solve the quantum scattering problem - find the scattered wave which result from an incident plane wave. You can do this by the method of partial waves - the analogous three dimensional problem is discussed in most quantum textbooks. You should find that only the  $m = 0$  partial wave contributes for small  $a$ . Following the discussion above, show that the diffraction constant is

$$d = \frac{2\pi}{\log\left(\frac{2}{ka}\right) - \gamma_e + i\frac{\pi}{2}} \quad (37.28)$$

where  $\gamma_e = 0.577 \dots$  is Euler's constant. Note that in this limit  $d$  depends weakly on  $k$  but not on the scattering angle.

(N. Whelan)

37.3. **Several diffractive legs.** Derive equation (37.18). The calculation involves considering slight variations of the diffractive orbit as in the simple case discussed above. Here it is more complicated because there are more diffractive arcs - however you should convince yourself

that a slight variation of the diffractive orbit only affects one leg at a time.

(N. Whelan)

37.4. **Unsymmetrized dynamical zeta function.** Assume you know nothing about symmetry decomposition. Construct the three node Markov diagram for figure 37.1 by considering  $A$ ,  $B$  and  $B'$  to be physically distinct. Write down the corresponding dynamical zeta function and check explicitly that for  $B = B'$  it factorizes into the product of the even and odd dynamical zeta functions. Why is there no term  $t_2$  in the full dynamical zeta function?

(N. Whelan)

37.5. **Three point scatterers.**

Consider the limiting case of the three disk game of pinball of figure 1.1 where the disks are very much smaller than their spacing  $R$ . Use the results of exercise 37.2 to construct the desymmetrized dynamical zeta functions, as in sect. 19.6. You should find  $1/\zeta_{A_1} = 1 - 2t$  where  $t = de^{i(kR - 3\pi/4)}/\sqrt{8\pi kR}$ . Compare this formula with that from chapter 10. By assuming that the real part of  $k$  is much greater than the imaginary part show that the positions of the resonances are  $k_n R = \alpha_n - i\beta_n$  where  $\alpha_n = 2\pi n + 3\pi/4$ ,  $\beta_n = \log(\sqrt{2\pi\alpha_n}/d)$  and  $n$  is a non-negative integer. (See also reference [11].)

(N. Whelan)

## References

- [37.1] A. Wirzba, CHAOS 2, 77 (1992);  
 [37.2] G. Vattay, A. Wirzba and P. E. Rosenqvist, Phys. Rev. Lett. 73, 2304 (1994); G. Vattay, A. Wirzba and P. E. Rosenqvist in *Proceedings of the International Conference on Dynamical Systems and Chaos: vol. 2*, edited by Y. Aizawa, S. Saito and K. Shiraiwa (World Scientific, Singapore, 1994).  
 [37.3] H. Primack, H. Schanz, U. Smilansky and I. Ussishkin, Phys. Rev. Lett. 76, 1615 (1996).  
 [37.4] N. D. Whelan, Phys. Rev. E 51, 3778 (1995).  
 [37.5] N. Pavloff and C. Schmit, Phys. Rev. Lett. 75, 61 (1995).  
 [37.6] M. Sieber, N. Pavloff, C. Schmit, Phys. Rev. E 55, 2279 (1997).